Surface & Coatings Technology

Experimental study of coated tools effects in dry cutting of natural fiber reinforced plastics

Faissal Chegdani *, Sabeur Mezghani, Mohamed El Mansori

Arts et Métiers ParisTech, MSMP-EA7350, Rue Saint Dominique, BP 508, 51006 Châlons-en-Champagne, Cedex, France

Keywords:
Natural fiber reinforced plastics
Profile milling
Tool coating
Tool wear
Multiscale surface analysis

A B S T R A C T

This work aims to investigate the tribological effects of coated tools on the surface finish of natural fiber reinforced plastics (NFRPs) during profile milling process with particular emphasis on the natural fiber cutting mechanisms and tool wear. Both up-milling and down-milling configurations were considered. The cutting experiments were carried out on unidirectional flax fibers reinforced polypropylene resin (UDF/PP) using three different cutting tools. Uncoated tungsten carbide, titanium diboride (T_iB_2) coated and diamond coated were used to conduct profile milling tests. Tribological cutting contacts were evaluated by measuring the specific cutting energy. Surface state was acquired by a scanning electronic microscope (SEM) and an optical microscope (OM). Surface topography was measured using a 2D Surfascan stylus profilometer. Machined NFRP surface finish was characterized using standard and multiscale analysis based on wavelets transform.
Results show that the cutting edge radius made by tool coating has a significant effect on surface finish. Natural fiber shearing is more efficient once the removed chip thickness exceeds the cutting edge radius value. Moreover, it had been demonstrated that the pertinent scales for surface finish analysis are between 50 μm and 1 mm which correspond to the multiscale fiber reinforcement structure. Furthermore, and unlike the uncoated tool, T_iB_2 and diamond coatings allow a good wear resistance of the cutting tools against the tribological solicitations of flax composite machining.

1. Introduction

Natural fiber reinforced plastics (NFRPs) constitute a real challenge for academia and industry since they are becoming a real substitute to synthetic fiber composites in several industrial applications which not require high structural performances [1–5]. Many factors engage the use of natural fibers in composite industry, such as the low production cost, the good mechanical properties, the valorization of local resources and the enhancement of materials and technologies taking into account the environmental impacts and the sustainable development [6,7].

Machining of composites such as milling process is an essential operation to facilitate the parts assembly in addition to the finishing of final products [8]. However, it's a complicated operation because of the heterogeneity in the internal structure of composite materials [9]. For all these raisons, many scientific studies are interested in machining of synthetic fiber composites to address the effect of process parameters, fiber orientation, and tool coating [10–17].

In the case of NFRP, these machining operations require the scientific understanding of the tribo-contact nature between the cutting tools and the different phases that are present inside the NFRP regarding the process parameters, the natural fiber structure and the tool properties. Unfortunately, the few studies that have addressed these issues have remained focused on the overall influence of process parameters on cutting forces, delamination factor and the global surface roughness of NFRP by using the statistical analysis of variance (ANOVA). The main outcome of these studies is that the feed rate has the larger contribution to the machining response [18–27]. Indeed, cutting forces, delamination factor and global surface roughness increase by feed rate increasing. Moreover, some comparative studies [24,26] between NFRP and glass fiber reinforced plastics (GFRP) show that the machining of NFRP generates low cutting forces but high delamination factor comparing to GFRP. However, standard surface roughness reveals a similar behavior between GFRP and NFRP that include high natural fiber stiffness [20]. Thus, previous work of the authors [28] addressed the multiscale influence of the natural fiber type (particularly the fiber stiffness) on the tribological behavior of NFRP during profile milling process. This study showed that the effect of fiber type is more relevant at fiber bundle scales and the machined surface roughness level decreases linearly by fiber stiffness increasing at this scale range. This proves that natural fiber type has an influence on the contact stiffness during the NFRP/tool interaction. Nevertheless, natural fiber structure and stiffness are not the only factors that control the cutting contact stiffness. Indeed, the effect of tool properties, such as the tool coating, can have a significant impact on the tribological performances during machining of NFRP by affecting the cutting edge surface properties and the edge radius.

* Corresponding author.
E-mail address: faissal.chegdani@ensam.eu (F. Chegdani).

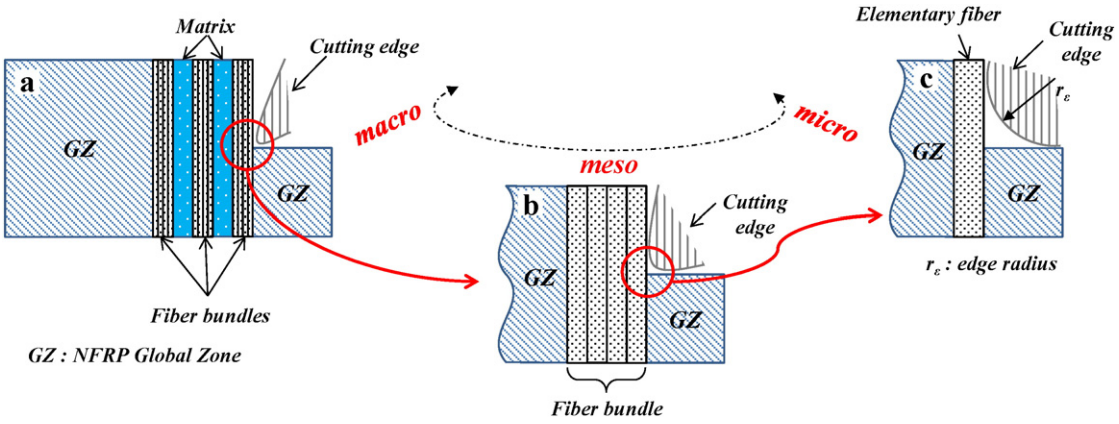

Fig. 1. Principal cutting scales for NFRP. a) Macroscopic scale. b) Mesoscopic scale. c) Microscopic scale.

Then, this paper purposes the study of the multiscale effect of coated cutting tools on the NFRP surfaces after profile milling process. The tribo-energetic approach [28–30] was used to reveal the physical cutting mechanisms that are related to the tribological contributions of both coating and machining parameters. The multiscale approach [28,31,32] was hence used to identify the effect of the cutting contact conditions on the machined NFRP surface quality. The idea is to take into account the cutting scale related to the machining parameters. The induced machining damages on both the NFRP workpieces and the coated tool have also been investigated.

2. Material and methods

2.1. Multiscale NFRP cutting structure

The understanding of NFRP cutting behavior is difficult due to the complex structure of the natural fibers inside the composite materials. Fig. 1 shows that machining the NFRP is extremely dependent on the analysis scale because it's directly related to the physical cutting scale between the tool and the natural fibers. Indeed, at microscopic scale, the cutting contact is between the tool edge and the elementary fiber (Fig. 1(c)) which has a high mechanical properties assured by the microfibrilar cellulosic structure along the fiber axis [33,34]. At the mesoscopic scale, the cutting contact is between the tool edge and the fiber bundle (Fig. 1(b)) because the natural fibers are gathered in bundles of elementary fibers and the bundle cohesion is insured by pectin interfaces that have a very low mechanical performance [35]. This construction causes a significant decrease of the mechanical properties of the fiber bundle comparing to the single elementary fiber in terms of stiffness and strength [36]. At the macroscopic scales, the cutting contact is between the tool edge and the composite structure that include the fiber bundles and the polymer matrix (Fig. 1(a)). The macroscopic composite structure is characterized by another decrease of the mechanical properties because of the low properties of the polymer matrix [37,38]. Consequently, the analysis of the physical cutting interactions cannot be made without taking into account the real cutting scale.

2.2. Coated cutting tools

Three iso-geometry helical carbide end mills with 10 mm of diameter and composed of two cutting edges with 30° of helix angle were provided by "*Sandvik Coromant — FR*" with different coating properties. Uncoated tungsten carbide (H10F), monolayer physical vapor deposition (PVD) titanium diboride (T_iB_2) coated (A4CA) and multilayer chemical vapor deposition (CVD) diamond coated (A4BX) are considered. Fig. 2 shows that each coating type generates different cutting edge sharpness. Table 1 summarizes the cutting tool characteristics. The edge radius of each cutting tool was measured using a 2D Surfascan stylus profilometer.

PVD coating process is made using sputter technology. During sputtering, the parts in the vacuum chamber for coating are first heated. Then, they are etched by bombardment with argon ions. This makes the metal surface pure and clean from any atomic contamination. A high negative voltage is then applied to the sputtering sources which contain the coating material. The resulting electrical gas discharge leads to the formation of positive argon ions that are accelerated in the direction of the coating material, which is atomized by the bombardment. The evaporated particles of atomized metal react with a gas that is introduced to the chamber and contains the component of the hard coating to be deposited. In traditional processes, the coating material must be melted. This inevitably creates droplets that form defects in the coating

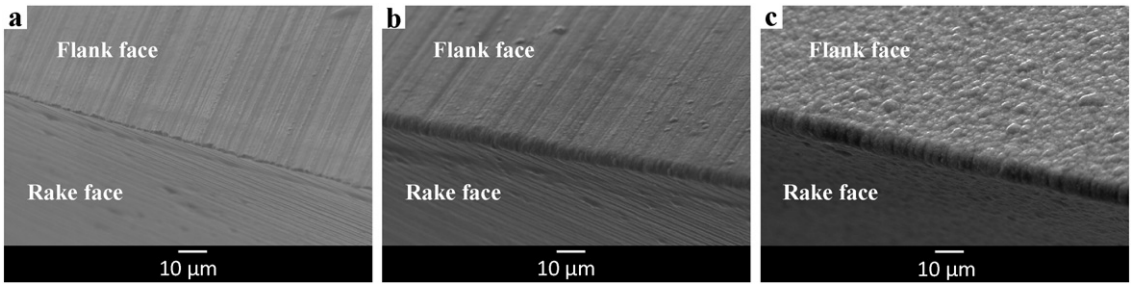

Fig. 2. SEM images of the cutting edge for each coated cutting tool: a) H10F, b) A4CA and c) A4BX.

Table 1
Coating characteristics of each studied cutting tool.

	H10F	A4CA	A4BX
Substrate	WC	WC	WC
Coating process	–	Monolayer PVD	Multilayer CVD
Coating composition	–	TiB_2	Diamond sp^3
Coating thickness (μm)	–	$2^{\pm 0.7}$	$7^{\pm 1}$
Hardness (HV)	1600	4000	10,000
Measured edge radius (μm)	$5.3^{\pm 0.6}$	$7.5^{\pm 0.5}$	$11.3^{\pm 0.7}$

Table 2
mechanical properties of the NFRP samples and their constituents.

	Flax fiber	PP matrix	UDF/PP
Tensile modulus (GPa)	50	0.93	17.6
Tensile strength (MPa)	500	29.5	109
Maximum strain	2%	14%	1.3%

structure and lead to a very rough surface. During sputtering, these droplets do not appear and the coating surface still smooth (Fig. 2(b)).

CVD technology is used to produce diamond coating using the hot filament process where the diamond is produced from gas. In H_2-C_xH_y gas atmosphere, carbon is turned into pure, crystalline diamond in a vacuum. This can produce up to four carat diamond per hour. It can be deposited as a micro-crystalline, nano-crystalline or multilayer coating. Multilayer technology ensures maximum stability by interlocking the individual layers within the coating. CVD diamond coating used in this study is a multilayer micro-crystalline coating (Fig. 2(c)).

2.3. Unidirectional flax/polypropylene composite workpieces

NFRP workpieces (Fig. 3(a)) used in this study are supplied by "*Composites Evolution — UK*". They are composed of unidirectional long flax fibers and polypropylene matrix (UDF/PP) as continuous warp flax yarns that are maintained in the longitudinal direction by synthetic weft yarns (Fig. 3(b)). Warp yarns are commingled flax/PP with 40% *vt* of UDF and 60% *vt* of PP (approximately 50% *wt* for each constituent). The warp yarn diameter is approximately 1 mm. The weft yarns are composed of co-polyamide/polyester co-spun. The incidence of weft yarns is 1 yarn per 2.5 mm (Fig. 3(b)), giving an areal weight of 14 g/m^2 (approximately 5% of the total fabric). Table 2 summarizes the mechanical properties of each constituent as provided by the supplier.

2.4. Cutting tests

Profile milling experiments were performed on instrumented DMU60 monoBLOCK® five axes CNC machine by testing two cutting configurations which are the up-milling and the down-milling as described in Fig. 3(b and c). Experimental system was mounted on a Kistler dynamometer (type 9255B) in order to measure the cutting forces. Tests have been conducted on dry cutting contact conditions at different feed rates. All other cutting parameters were kept constant. The milling process parameter values are presented in Table 3. In order to get reliable results, each test was repeated three times under identical conditions and with a new cutting tool at each time.

Geometrical and superficial variations of each workpiece samples have been measured at five locations using a 2D Surfascan stylus profilometer according to the ISO4287 standard. The tip radius of the diamond stylus is 2 μm. The surface micro-profile on each specimen was taken along the machining direction over a sampling length of 2 μm. The evaluation length is 16.8 mm and a cut-off of 0.8 mm is used to evaluate the arithmetic mean deviation of roughness (R_a) profile parameter. Microscopic observations of UDF/PP surface state were made by a scanning electron microscope (SEM) (JSM — 5510LV) at low vacuum mode. Typical representative surface morphology as induced by milling of each experimental configuration was taken into account for the microscopic analysis. Milled surface defects were evaluated by an optical microscope (Nikon SMZ — 10).

3. Results and discussion

3.1. Natural fiber cutting mechanisms

In order to understand the effect of tool coating on the cutting mechanisms of flax fibers inside the NFRP, the specific cutting energy was calculated from cutting forces [28] for each cutting test configuration. Fig. 4 shows that the up-milling specific cutting energy (Fig. 4(a)) is less than the down-milling specific cutting energy (Fig. 4(b)); especially at low

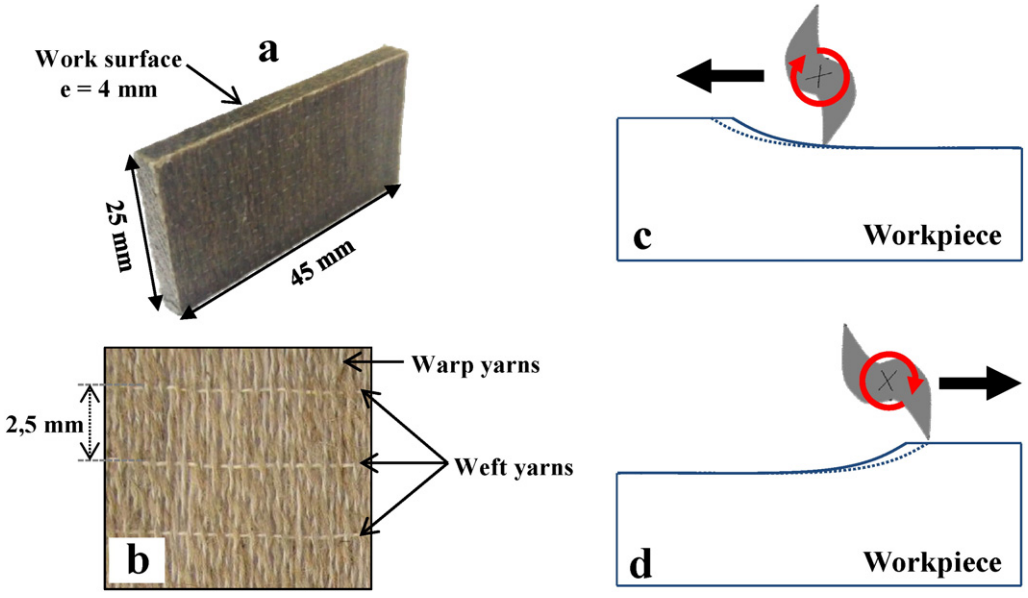

Fig. 3. a) Photograph of the workpiece sample showing the worksurface. b) Structure of the flax fiber reinforcement. c) Schematization of the up-milling configuration. d) Schematization of the down-milling configuration.

Table 3
Process parameters used for the profile milling tests.

Milling configuration	Feed (mm/tooth)	Cutting speed (m/min)	Depth of cut (mm)
Up-milling	0.005	100	1
Down-milling	0.01		
	0.02		
	0.04		
	0.08		
	0.16		

and medium feed rates. At high feed rates, the energetic results become similar between the three cutting tools and also between the two cutting configurations. Indeed, the cutting conditions are favorable at high feed rates as these latter satisfy the concept of the minimum chip thickness when the undeformed chip thickness is much higher than the minimum chip thickness [39].

Energetic analysis of Fig. 4 indicates that the fiber shearing is more easily achieved by the up-milling configuration than by the down-milling configuration. This can be explained by the fiber maintaining during the NFRP/tool cutting contact as described in Fig. 5. At the up-milling configuration, the fibers to be cut are well supported by the forward material as shown in Fig. 5(b). This configuration increases the fiber contact stiffness and allows the fibers to be sheared more easily. At down-milling configuration, the maintenance of the fibers to be cut is insured by the behind material which is insufficient for supporting the cutting contact interaction as described in Fig. 5(a).

Moreover, Fig. 4 shows that the coated tool effects are more obvious at up-milling configuration between low and medium feed rates (Fig. 4(a)). In fact, H10F tool generates the lowest specific energy, followed by the A4CA tool. The A4BX tool induces the highest specific energy. This can be explained by the cutting edge radius for each tool produced by the coating process. The uncoated tool (H10F) has the lowest edge radius, followed by T_iB_2 PVD coated tool (A4CA) and the diamond CVD coated tool (A4BX) as shown in Fig. 2 and Table 1. Indeed, it's well known that the more the cutting edge radius is high, the more plastic deformation and sliding mechanisms contribute to the cutting energy, especially when the tool edge radius comes to be on the order of the undeformed chip thickness [40]. Consequently, low cutting edge radius leads to reducing both the sliding and the plastic deformation components and favors the fiber shearing mechanism (i.e. reducing the specific cutting energy).

It can be concluded that both up-milling configuration and low cutting edge radius favor the shearing mechanism of the natural fibers, while both down-milling configuration and high edge radius favor the plastic deformation and the springback of the natural fibers after the milling operation. However, neither up-milling nor down-milling configurations cannot exhibit a pure fiber shearing because of the high flexibility of the natural fibers as they are soft by nature [41]. Consequently, the natural fibers have a significant ability to be easily deformed in contact with the cutting edge. This will favor the plastic deformation rather than shearing of the fiber during the milling operation.

3.2. Multiscale surface finish analysis

Standard surface roughness analysis has been developed by measuring the arithmetic mean roughness criterion R_a after the profile milling process.

Fig. 6 presents the standard surface roughness for both up-milling and down-milling configurations at all the feed rate range. It shows that roughness increasing level for the down-milling configuration (Fig. 6(b)) is strongly higher than that of the up-milling configuration (Fig. 6(a)), especially at low and medium feed rates. The roughness level becomes similar between the two cutting configurations at the high feed rates for the same raisons discussed in Section 3.1.

Furthermore, A4BX cutting tool induces the highest roughness level, followed by the A4CA then H10F. This demonstrates the functional relationship between the cutting edge radius generated by the tool coating and the induced surface roughness. Indeed, Fig. 7 presents the microscopic states of the milled surfaces generated by the three cutting tool at low, medium and high feed rates. It shows that, effectively, increasing the cutting edge radius increases the uncut fiber extremities that exceed the machined surface. However, increasing the feed rate reduces these uncut fiber extremities. Since these latter are the main responsible of the surface roughness increase [28], it can be concluded that increasing the cutting edge radius increases the surface roughness and increasing the feed rate reduces the surface roughness. It's important to note that the effect of the roughness of coated tools (Fig. 2) was not considered as it will not leave its mark on the milled surface because of the exceeded fibers.

For more understanding of the relationship between the milled surface roughness, cutting parameters and the cutting edge radius induced by tool coating, multiscale analysis of the milled surface topography was made using the multiscale decomposition approach. More details about this multiscale analysis method can be found in [28]. Multiscale surface roughness analysis was performed using the multiscale roughness spectrum (M_a(i)) by calculating the arithmetic mean roughness deviation (M_a) at each scale "*i*" of the decomposition.

At this step of study, the mean chip thickness will be used instead of the feed rate to evaluate the multiscale surface roughness in terms of the removed material quantity. The mean chip thickness (h_m) can be computed from the feed rate (f_z) in the case of profile milling process using the Eq. (1) [42]. Where a_e and ϕ are the depth of cut and the tool diameter, respectively. The corresponding chip thickness values of each feed value are presented in Table 4.

$$h_m = f_z \times \sqrt{\frac{a_e}{\phi}}. \tag{1}$$

Fig. 8 shows that the roughness is at its minimum at the smallest scale ($i = 16$ μm) which refers to the elementary fiber diameter scales (between 10 and 20 μm). Both the feed and the cutting edge radius don't significantly affect this minimum roughness as it seems to be similar for all the experimental configurations. In fact, the elementary fiber presents in this microscopic scale has a very high

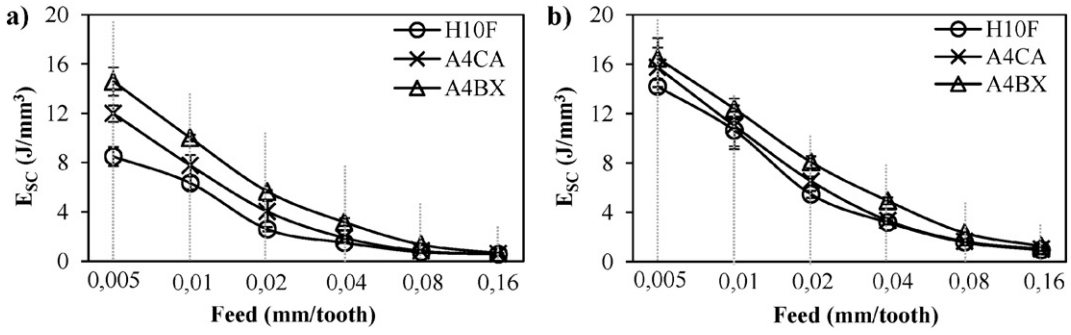

Fig. 4. Specific cutting energy for profile milling process. a) Up-milling configuration. b) Down-milling configuration.

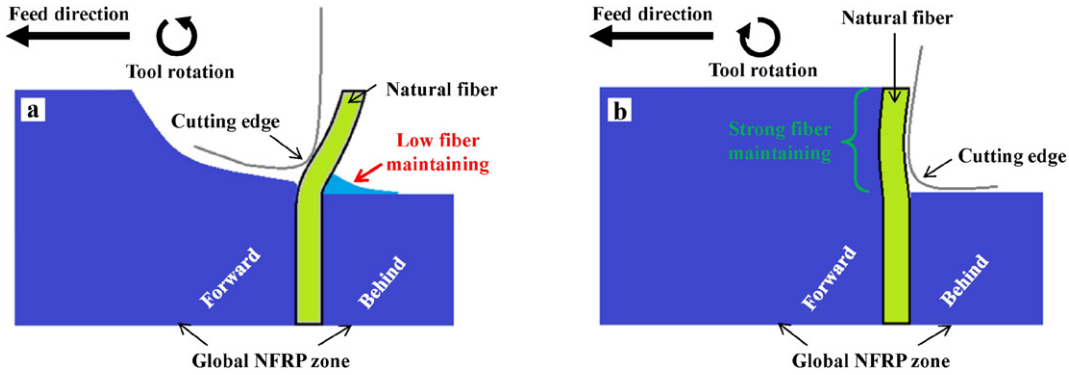

Fig. 5. Schematization of the natural fiber behavior during milling operation. a) Down-milling configuration. b) Up-milling configuration.

mechanical properties comparing to the polymer matrix as shown in Table 2. The high elementary fiber stiffness controls the cutting contact stiffness and, then, the effects of the feed and the edge radius are not obvious. The roughness level increases significantly by increasing the analysis scale until the scale $i = 1$ mm where the roughness level reaches its maximum. Indeed, the more the analysis scale increases, the more additional elementary fibers are taken into account in the cutting scale until reaching the fiber bundles (Fig. 1(b)). The stiffness drop from the elementary fiber to the fiber bundle (Section 2.1) causes a significant decrease in the cutting contact stiffness between the cutting edge and the fibers. This will reduce the fiber shearing efficiency and, consequently, generates an important roughness increasing. Consequently, at these high roughness levels, the impact of feed (or chip thickness) and cutting edge radius will be more obvious.

The multiscale analysis demonstrates the importance of considering the analysis scale which is undeniably linked to the cutting scale as explained in Section 2.1. Therefore, the pertinent scales to analyze the both cutting edge radius and chip thickness effect on machined surface quality of UDF/PP are, according to the Fig. 8, between 50 μm and 1 mm. Physically, the scale $i = 50$ μm corresponds to the minimum diameter of technical flax fiber [43] while the scale $i = 1$ mm refers to the flax yarn diameter (Section 2.3).

By analyzing the M_a spectrums of each milling configuration between 50 μm and 1 mm, Fig. 8 reveals that, globally, there is a functional relationship between the edge radius induced by the tool coating and the mean chip thickness. Indeed, the M_a spectrums present two different behaviors in terms of both chip thickness (h_m) values and edge radius (r_ε) values:

- When $h_m < r_\varepsilon$: The surface roughness presents its highest levels and decreases significantly by chip thickness increasing because we are in the unfavorable cutting conditions that favor sliding and plastic deformation as explained in Section 3.1.
- When $h_m > r_\varepsilon$: The effect of chip thickness becomes insignificant and the surface roughness level reaches its minimum as the favorable cutting conditions are achieved.

It can be concluded, by the standard and the multiscale surface analysis, that reducing the surface roughness (i.e. activating the natural fiber shearing mechanism) amounts to be achieved by the feed rates which can generate chip thicknesses higher than the edge radius of the cutting tool (i.e. to be in the favorable cutting conditions as explained in Section 3.1).

It's interesting to note the insignificance of the tool hardness on the profile milling results regarding the energetic analysis and the surface roughness. Indeed, even if there is an important difference of the hardness values between the three studied cutting edges (Table 1), this hardness difference cannot influence the cutting results because of the very low hardness of the UDF/PP workpieces that can be negligible compared with that of the cutting tools. The UDF/PP hardness has been measured and it is around 11 HV. Then, a significant changing of cutting tool hardness seems to be not able to affect the cutting interaction and cutting mechanisms.

3.3. Induced machining defects

3.3.1. Fluffing defect

Fluffing is among the most known defects in composite processing industry. Fluffing of flax fibers is observed at both top and bottom edges of milled surface as shown in Fig. 9. The top fluffing (Δx) corresponds to the fluffing defect produced by the exit of the cutting edge. The bottom fluffing (Δy) corresponds to the fluffing defect produced by the entry of the cutting edge. Thus, Δx and Δy, which correspond respectively to the uncut fibers length at the top and the bottom edges of milled surface, were measured after each test using the optical microscope.

Fig. 9 shows that the fluffing defect is more apparent at the top edge of the milled surface (i.e. the exit of the cutting edge). The down-milling

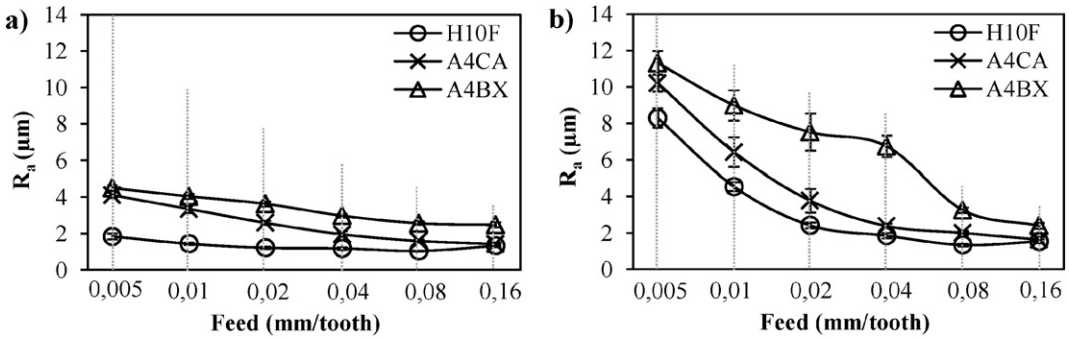

Fig. 6. Standard surface roughness after profile milling process of UDF/PP. a) Up-milling configuration. b) Down-milling configuration.

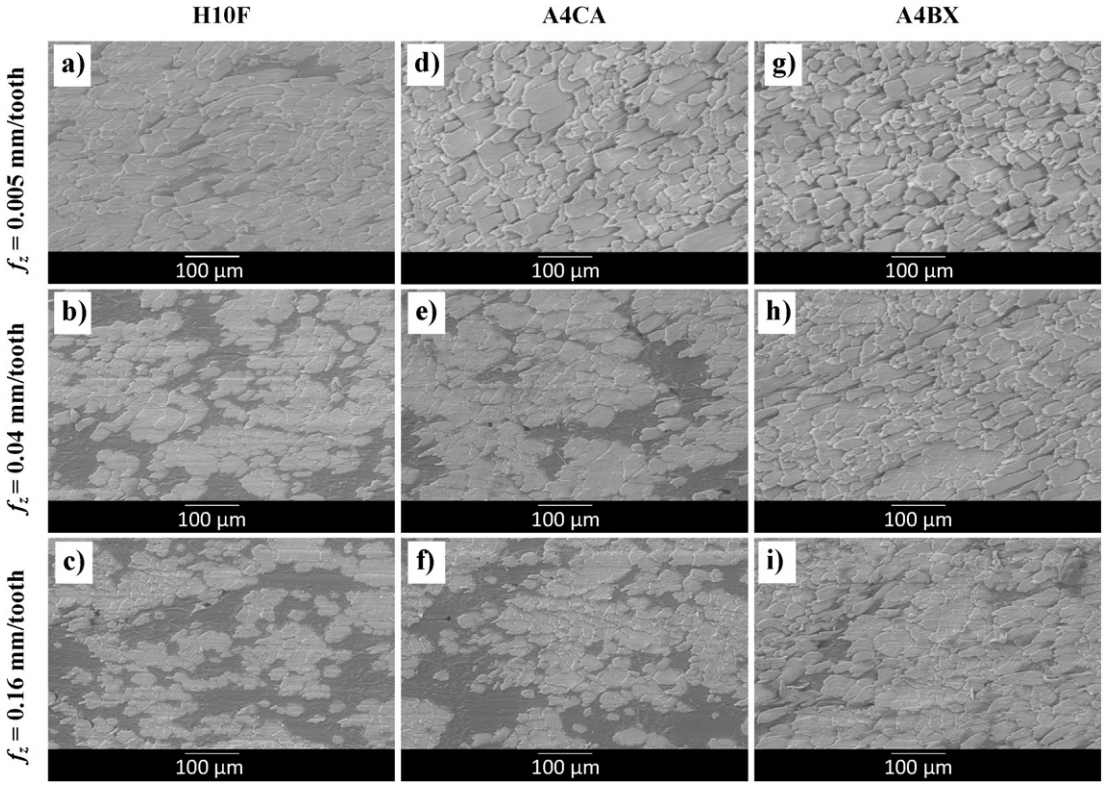

Fig. 7. SEM images showing the microscopic surface quality after up-milling process with the three different coating properties.

configuration generates more fluffing defect than the up-milling configuration. Moreover, the effect of the cutting edge radius on the fluffing length is more obvious at up-milling configuration in which the A4BX tool (i.e. the highest cutting edge radius) causes the highest fluffing length. The H10F tool (i.e. the lowest cutting edge radius) causes the lowest fluffing length.

The fluffing defect can also be explained by the fiber maintaining aspect (Section 3.1). Indeed, the natural fibers that are present at the two extreme edges of the milled surface did not have a sufficient maintaining during the cutting operation and they tend to deform more than those present inside the composite. In addition, increasing the cutting edge radius favors the fiber deformation more than the fiber shearing. Then, increasing the cutting edge radius for the fibers at the two extreme edges of the worksurface will greatly reduce their shearing efficiency (i.e. increasing the uncut fiber extremities at the two edges of the milled surface).

3.3.2. Tool wear

Due to the non-abrasive character of natural fibers that participates in a slow wear evolution of the cutting tools comparing to the synthetic fibers [41], no wear was detected after the profile milling tests. Then, each cutting tool has been engaged to conduct an accelerated cyclic machining of a UDF/PP workpiece. 50 milling cycles were consecutively done for each cutting tool. Each milling cycle was realized on 200 mm of UDF/PP cutting length with 100 m/min of cutting speed and 32 mm/min of feed speed. Thus, each wear test took approximately 5 h.

Cutting tool wear has been investigated by SEM observations and cutting edge radius measurement after the accelerated wear tests in order to compare them with the initial measurements of Table 1. After the wear test, no wear appearance was detected by the SEM observations on the cutting edge of the T_iB_2 coated (A4CA) and the diamond coated (A4BX) tools. Only the uncoated tool (H10F) shows the signs of wear at the tip of the cutting edge as shown in Fig. 10. Indeed, Fig. 10(b) shows that, after the accelerated wear test, significant microcracks at the tip of the cutting edge was detected but no surface structure modification of the flank face was observed. This can be due to the mechanical damage (subsurface damage, microcracks, …) induced by the manufacturing process of the cutting tools and, especially, the finishing process of the cutting edge which causes an initial microcracks at the tip of the cutting edge (Fig. 10(a)). According to Fig. 10(c), only the H10F cutting edge radius increased. This proves, effectively, the presence of wear at the tip the H10F cutting edge. Therefore, the milled surface roughness can increase with time as the cutting edge radius increases with time because of wear.

It can be concluded that coating allows the avoiding of wear initiation at the tip of the cutting edge when milling UDF/PP. Introducing hard coating (like T_iB_2 or diamond) to tungsten carbide cutting edge can protect it against the strictest solicitations in this sensitive area of the cutting tool thanks to their high hardness presented in Table 1. This can let the induced surface roughness constant with time until the wear initiation of the coating.

Table 4
Equivalent chip thickness values for the different feed values.

Feed (mm/tooth)	0.005	0.01	0.02	0.04	0.08	0.16
Chip thickness (µm)	1.6	3.2	6.4	12.8	25.6	51.2

4. Conclusion

The effect of coated tools on the UDF/PP profile milling performances had been investigated in this study by comparing the cutting behaviors of uncoated tungsten carbide tool with both T_iB_2 coated and diamond coated tools. This study was conducted at dry cutting conditions by testing both the up-milling and the down-milling configurations. The following conclusions can be drawn:

- Up-milling configuration is more suitable than down-milling configuration for the profile milling of UDF/PP at low and medium feed rates. Up-milling configuration favors the shearing mechanism of the flax

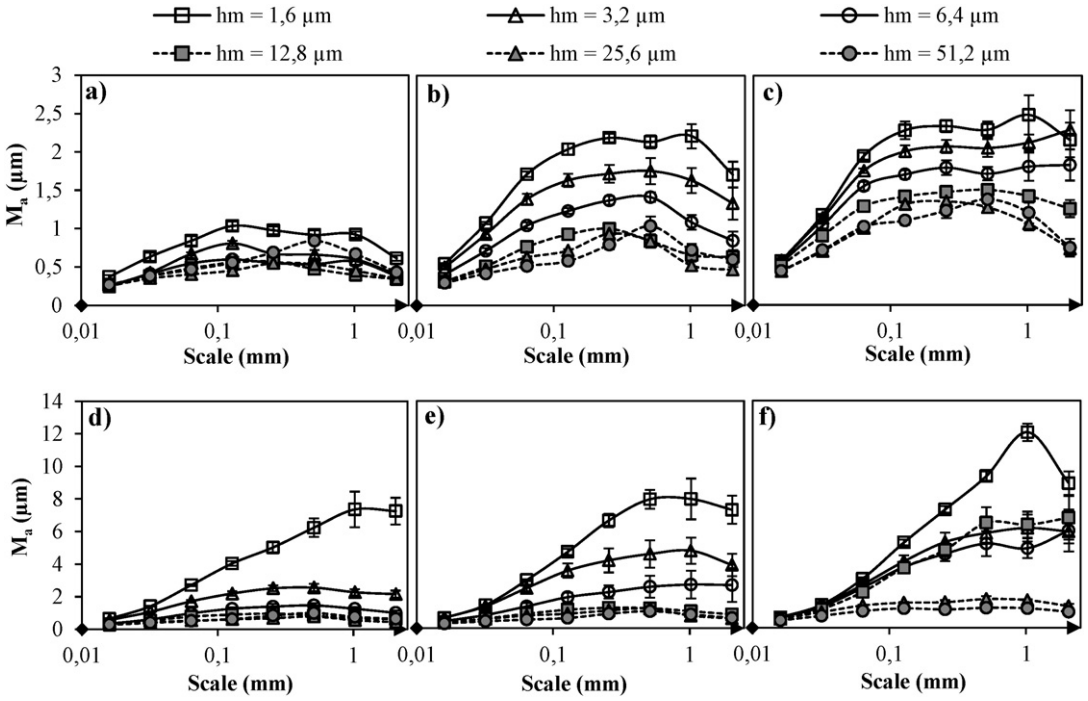

Fig. 8. Multiscale surface roughness of milled UDF/PP. a) Up-milling by H10F. b) Up-milling by A4CA. c) Up-milling by A4BX. d) Down-milling by H10F. e) Down-milling by A4CA. f) Down-milling by A4BX.

fibers thanks to the high fiber maintaining during the cutting operation. The fiber maintaining is very low at the extreme edges of the worksurface which causes fluffing defects.

- Both T_iB_2 and diamond coatings increase the cutting edge radius. Consequently, increasing the cutting edge radius favors the plastic deformation of flax fibers, in addition to their springback, when interacting with the cutting tool. Then, increasing the cutting edge radius increases the milled surface roughness.
- Multiscale analysis demonstrates the significance of taking into account the analysis scale. For the UDF/PP milling, the pertinent scales to evaluate the surface topography of the milled surface roughness are between 50 µm and 1 mm. These scales are, typically, between the technical fiber diameter and the yarn diameter. Moreover, multiscale analysis confirmed the relationship between the cutting edge radius and the mean chip thickness. Thus, the shearing mechanism is activated when the chip thickness is higher than the cutting edge radius.
- Only the uncoated tool shows signs of wear on the tip of the cutting edge in form of microcracks. This damage causes a significant increasing of the cutting edge radius and then a surface roughness increasing of the NFRP with time. The non-abrasive nature of flax fibers does not affect the coating structure of both T_iB_2 and diamond which have a high hardness. Then, the choice of the cutting tool for machining the NFRP composites requires a good compromise between the cutting edge sharpness and the tool coating. This will provide an efficient natural fiber cutting associated with long tool life.

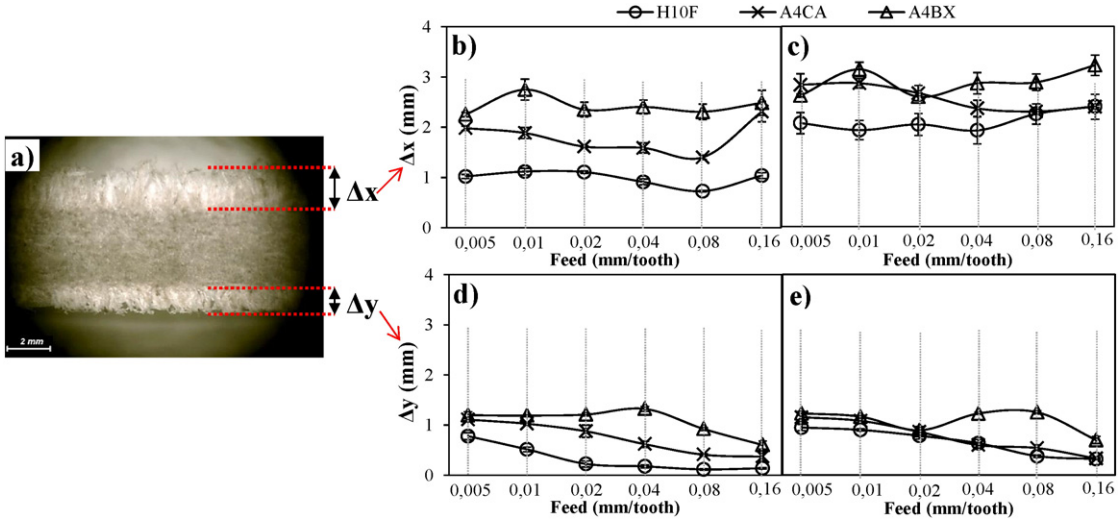

Fig. 9. a) Optical microscope image showing the top fluffing (Δx) and the bottom fluffing (Δy). b) Top fluffing of up-milled surfaces. c) Top fluffing of down-milled surfaces. d) Bottom fluffing of up-milled surface. e) Bottom fluffing of down-milled surfaces.

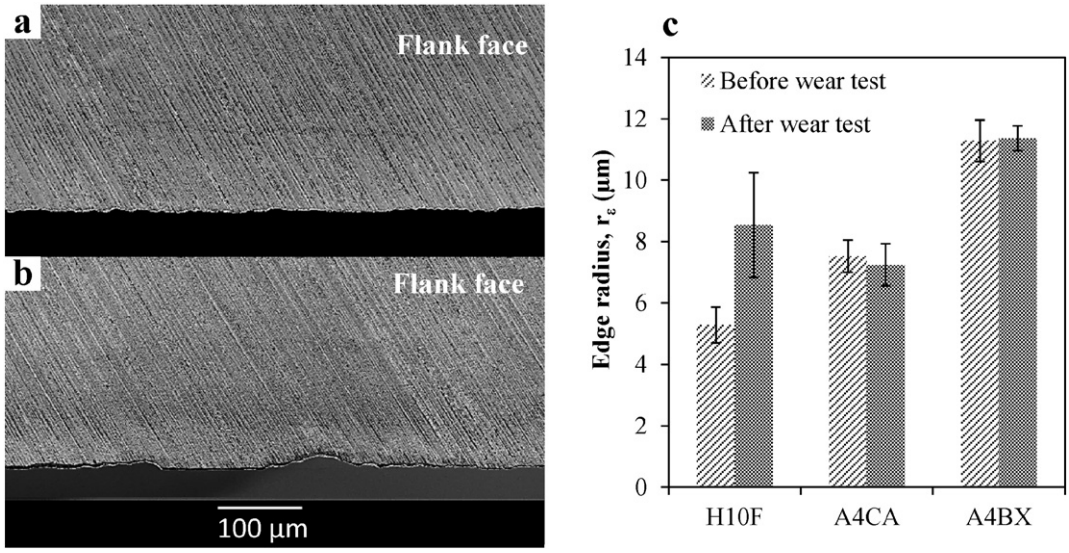

Fig. 10. a) SEM micrographs of the active zone of the H10F cutting edge before wear test and b) after wear test. c) Cutting edge radius values of the milling tools before and after the wear test.

Acknowledgments

The authors acknowledge the urban community of Châlons-en-Champagne (*Cités en Champagne*) for their financial support.

References

[1] D.B. Dittenber, H.V.S. GangaRao, Critical review of recent publications on use of natural composites in infrastructure, Compos. Part A Appl. Sci. Manuf. 43 (2012) 1419–1429, http://dx.doi.org/10.1016/j.compositesa.2011.11.019.
[2] O. Faruk, A.K. Bledzki, H.-P. Fink, M. Sain, Biocomposites reinforced with natural fibers: 2000–2010, Prog. Polym. Sci. 37 (2012) 1552–1596, http://dx.doi.org/10.1016/j.progpolymsci.2012.04.003.
[3] M. John, S. Thomas, Biofibres and biocomposites, Carbohydr. Polym. 71 (2008) 343–364, http://dx.doi.org/10.1016/j.carbpol.2007.05.040.
[4] D.U. Shah, Developing plant fibre composites for structural applications by optimising composite parameters: a critical review, J. Mater. Sci. 48 (2013) 6083–6107, http://dx.doi.org/10.1007/s10853-013-7458-7.
[5] P. Wambua, J. Ivens, I. Verpoest, Natural fibres: can they replace glass in fibre reinforced plastics? Compos. Sci. Technol. 63 (2003) 1259–1264, http://dx.doi.org/10.1016/S0266-3538(03)00096-4.
[6] A. Shalwan, B.F. Yousif, In state of art: mechanical and tribological behaviour of polymeric composites based on natural fibres, Mater. Des. 48 (2013) 14–24, http://dx.doi.org/10.1016/j.matdes.2012.07.014.
[7] A. Lefeuvre, A. Bourmaud, C. Morvan, C. Baley, Tensile properties of elementary fibres of flax and glass: analysis of reproducibility and scattering, Mater. Lett. 130 (2014) 289–291, http://dx.doi.org/10.1016/j.matlet.2014.05.115.
[8] J.P. Davim, P. Reis, Damage and dimensional precision on milling carbon fiber-reinforced plastics using design experiments, J. Mater. Process. Technol. 160 (2005) 160–167, http://dx.doi.org/10.1016/j.jmatprotec.2004.06.003.
[9] S. Abrate, D. Walton, Machining of composite materials. Part II: Non-traditional methods, Compos. Manuf. 3 (1992) 85–94, http://dx.doi.org/10.1016/0956-7143(92)90120-J.
[10] C.R. Dandekar, Y.C. Shin, Modeling of machining of composite materials: a review, Int. J. Mach. Tools Manuf. 57 (2012) 102–121, http://dx.doi.org/10.1016/j.ijmachtools.2012.01.006.
[11] L. Larbi, M. Nouari, M. El Mansori, Working parameters effects on machining-induced damage of fibre-reinforced composites: numerical simulation analysis, Int. J. Mater. Prod. Technol. 32 (2008) 136, http://dx.doi.org/10.1504/IJMPT.2008.018977.
[12] P. Ghidossi, M. El Mansori, F. Pierron, Edge machining effects on the failure of polymer matrix composite coupons, Compos. Part A Appl. Sci. Manuf. 35 (2004) 989–999, http://dx.doi.org/10.1016/j.compositesa.2004.01.015.
[13] P. Ghidossi, M. El Mansori, F. Pierron, Influence of specimen preparation by machining on the failure of polymer matrix off-axis tensile coupons, Compos. Sci. Technol. 66 (2006) 1857–1872, http://dx.doi.org/10.1016/j.compscitech.2005.10.009.
[14] A. Mkaddem, A. Ben Soussia, M. El Mansori, Wear resistance of CVD and PVD multilayer coatings when dry cutting fiber reinforced polymers (FRP), Wear 302 (2013) 946–954, http://dx.doi.org/10.1016/j.wear.2013.03.017.
[15] A. Ben Soussia, A. Mkaddem, M. El Mansori, Rigorous treatment of dry cutting of FRP — interface consumption concept: a review, Int. J. Mech. Sci. 83 (2014) 1–29, http://dx.doi.org/10.1016/j.ijmecsci.2014.03.017.
[16] R. Zitoune, F. Collombet, F. Lachaud, R. Piquet, P. Pasquet, Experiment-calculation comparison of the cutting conditions representative of the long fiber composite drilling phase, Compos. Sci. Technol. 65 (2005) 455–466, http://dx.doi.org/10.1016/j.compscitech.2004.09.028.
[17] A. Ben Soussia, A. Mkaddem, M. El Mansori, Effect of coating type on dry cutting of glass/epoxy composite, Surf. Coat. Technol. 215 (2013) 413–420, http://dx.doi.org/10.1016/j.surfcoat.2012.04.098.
[18] S.A.S. Azuan, P. Composites, Effects of drilling parameters on delamination of coconut meat husk reinforced, Adv. Environ. Biol. 7 (2013) 1097–1100.
[19] D. Babu, S. Babu, B.U.M. Gowd, Effects of machining parameters in the drilling of jute fiber reinforced plastic: evaluation of the delamination factor, Glob. J. Mech. Eng. Comput. Sci. 2 (2012) 57–62.
[20] G.D. Babu, K.S. Babu, B.U.M. Gowd, Effect of machining parameters on milled natural fiber-reinforced plastic composites, J. Adv. Mech. Eng. (2013) 1–12, http://dx.doi.org/10.7726/jame.2013.1001.
[21] G.D. Babu, K.S. Babu, B.U.M. Gowd, Effects of drilling parameters on delamination of hemp fiber reinforced composites, Int. J. Mech. Eng. Res. Dev. 2 (2012) 1–8.
[22] P.K. Bajpai, I. Singh, Drilling behavior of sisal fiber-reinforced polypropylene composite laminates, J. Reinf. Plast. Compos. 32 (2013) 1569–1576, http://dx.doi.org/10.1177/0731684413492866.
[23] D. Chandramohan, K. Marimuthu, Drilling of natural fiber particle reinforced polymer composite material, Int. J. Adv. Eng. Res. Stud. I (2011) 134–145.
[24] L.M.P. Durão, D.J.S. Gonçalves, J.M.R.S. Tavares, V.H.C. de Albuquerque, T.H. Panzera, L.J. Silva, et al., Drilling delamination outcomes on glass and sisal reinforced plastics, Mater. Sci. Forum 730–732 (2012) 301–306, http://dx.doi.org/10.4028/www.scientific.net/MSF.730-732.301.
[25] S. Jayabal, U. Natarajan, Drilling analysis of coir-fibre-reinforced polyester composites, Bull. Mater. Sci. 34 (2011) 1563–1567, http://dx.doi.org/10.1007/s12034-011-0359-y.
[26] P.N.E. Naveen, M. Yasaswi, R.V. Prasad, Experimental investigation of drilling parameters on composite materials, J. Mech. Civ. Eng. 2 (2012) 30–37.
[27] R. Vinayagamoorthy, N. Rajeswari, Analysis of cutting forces during milling of natural fibered composites using fuzzy logic, Int. J. Compos. Mater. Manuf. 2 (2012) 15–21.
[28] F. Chegdani, S. Mezghani, M. El Mansori, A. Mkaddem, Fiber type effect on tribological behavior when cutting natural fiber reinforced plastics, Wear 332–333 (2015) 772–779, http://dx.doi.org/10.1016/j.wear.2014.12.039.
[29] H.A. Abdel-Aal, M. Nouari, M. El Mansori, Tribo-energetic correlation of tool thermal properties to wear of WC–Co inserts in high speed dry machining of aeronautical grade titanium alloys, Wear 266 (2009) 432–443, http://dx.doi.org/10.1016/j.wear.2008.04.023.
[30] E. Sura, M. El Mansori, P. Ghidossi, S. Deblaise, T.D. Negro, H. Khanfir, An energy analysis of belt polishing process and its applications to time cycle and tracking effects, Mach. Sci. Technol. 11 (2007) 217–234, http://dx.doi.org/10.1080/10910340701340059.
[31] M. El Mansori, S. Mezghani, L. Sabri, H. Zahouani, On concept of process signature in analysis of multistage surface formation, Surf. Eng. 26 (2010) 216–223, http://dx.doi.org/10.1179/174329409X455412.
[32] S. Mezghani, M. El Mansori, A. Massaq, P. Ghidossi, Correlation between surface topography and tribological mechanisms of the belt-finishing process using multiscale finishing process signature, C. R. Méc. 336 (2008) 794–799, http://dx.doi.org/10.1016/j.crme.2008.09.002.
[33] C. Baley, Analysis of the flax fibres tensile behaviour and analysis of the tensile stiffness increase, Compos. Part A Appl. Sci. Manuf. 33 (2002) 939–948, http://dx.doi.org/10.1016/S1359-835X(02)00040-4.

[34] K. Charlet, C. Baley, C. Morvan, J.P. Jernot, M. Gomina, J. Bréard, Characteristics of Hermès flax fibres as a function of their location in the stem and properties of the derived unidirectional composites, Compos. Part A Appl. Sci. Manuf. 38 (2007) 1912–1921, http://dx.doi.org/10.1016/j.compositesa.2007.03.006.
[35] C. Morvan, C. Andème-Onzighi, R. Girault, D.S. Himmelsbach, A. Driouich, D.E. Akin, Building flax fibres: more than one brick in the walls, Plant Physiol. Biochem. 41 (2003) 935–944, http://dx.doi.org/10.1016/j.plaphy.2003.07.001.
[36] M.J.A. van den Oever, H.L. Bos, K. Molenveld, Flax fibre physical structure and its effect on composite properties: impact strength and thermo-mechanical properties, Angew. Makromol. Chem. 272 (1999) 71–76, http://dx.doi.org/10.1002/(SICI)1522-9505(19991201)272:1<71::AID-APMC71>3.0.CO;2-R.
[37] K. Charlet, J.-P. Jernot, M. Gomina, L. Bizet, J. Breard, Mechanical properties of flax fibers and of the derived unidirectional composites, J. Compos. Mater. 44 (2010) 2887–2896, http://dx.doi.org/10.1177/0021998310369579.
[38] G. Romhány, J. Karger-Kocsis, T. Czigány, Tensile fracture and failure behavior of thermoplastic starch with unidirectional and cross-ply flax fiber reinforcements, Macromol. Mater. Eng. 288 (2003) 699–707, http://dx.doi.org/10.1002/mame.200300040.
[39] J. Chae, S.S. Park, T. Freiheit, Investigation of micro-cutting operations, Int. J. Mach. Tools Manuf. 46 (2006) 313–332, http://dx.doi.org/10.1016/j.ijmachtools.2005.05.015.
[40] I.S. Kang, J.S. Kim, Y.W. Seo, Cutting force model considering tool edge geometry for micro end milling process, J. Mech. Sci. Technol. 22 (2008) 293–299, http://dx.doi.org/10.1007/s12206-007-1110-x.
[41] U. Nirmal, K.O. Low, J. Hashim, On the effect of abrasiveness to process equipment using betel nut and glass fibres reinforced polyester composites, Wear 290–291 (2012) 32–40, http://dx.doi.org/10.1016/j.wear.2012.05.022.
[42] G. Boothroyd, W.A. Knight, Fundamentals of Machining and Machine Tools, Taylor & Francis, 2006.
[43] H.L. Bos, K. Molenveld, W. Teunissen, A.M. van Wingerde, D.R.V. van Delft, Compressive behaviour of unidirectional flax fibre reinforced composites, J. Mater. Sci. 39 (2004) 2159–2168, http://dx.doi.org/10.1023/B:JMSC.0000017779.08041.49.